Tunneling Magnetoresistance with Sign Inversion in Junctions Based on Iron Oxide Nanocrystal Superlattices

Indira Chaitanya Lekshmi,[†] Raffaella Buonsanti,[†] Concetta Nobile,[†] Ross Rinaldi,[†,‡] Pantaleo Davide Cozzoli,[†,‡] and Giuseppe Maruccio[†,§,*]

[†]NNL CNR-Istituto Nanoscienze, Via per Arnesano, 73100 Lecce, Italy, [‡]Department of Innovation Engineering, and [§]Department of Physics, University of Salento, Via per Arnesano, 73100 Lecce, Italy

ABSTRACT Magnetic tunnel junctions sandwiching a superlattice thin film of iron oxide nanocrystals (NCs) have been investigated. The transport was found to be controlled by Coulomb blockade and single-electron tunneling, already at room temperature. A good correlation was identified to hold between the tunnel magnetoresistance (TMR), the expected magnetic properties of the NC arrays, the charging energies evaluated from current−voltage curves, and the temperature dependence of the junction resistance. Notably, for the first time, a switching from negative to positive TMR was observed across the Verwey transition, with a strong enhancement of TMR at low temperatures.

KEYWORDS: spintronics · magnetoresistance · Coulomb blockade · iron oxide · nanocrystals

The idea of pursuing spintronics with organic materials, molecular magnets, and/or magnetic inorganic nanocrystals (NCs) as building blocks is widely acknowledged as very promising.[1−18] In particular, integrating NCs with discrete energy levels[19,20] into spin nanodevices has attracted considerable interest due to expectation of novel properties/phenomena resulting from the interplay between spin-dependent and single-electron transport, as well as spin accumulation.[9,11,21] So far, magnetotransport through NCs has been investigated in vertical structures within granular systems prepared by sputtering or physical evaporation methods[12,22] or within superlattices made of self-assembled colloidal NCs.[23−26] Notably, in the latter case, collective magnetic properties due to interparticle interactions have been observed (*e.g.*, two-dimensional superlattices show squarer hysteresis loops relative to those of isolated NCs).[27,28] Such collective properties can be further modulated if NC self-assembly is promoted under the driving force of an externally applied magnetic field that leads to oriented dipoles over short- to long-distance ranges.[27,29−32]

Inverse spinel cubic iron oxide can occur in the ferrimagnetic Fe_3O_4 (magnetite) and γ-Fe_2O_3 (maghemite) phases that are featured by nearly identical lattice parameters ($a_{Fe_3O_4}$ = 8.35 Å and $a_{\gamma\text{-}Fe_2O_3}$ = 8.39 Å, respectively). Wet-chemically synthesized NCs are often reported to be characterized by a mixed composition of γ-Fe_2O_3 and Fe_3O_4 phases, the relative proportions of which depend upon the preparation conditions. NCs of these oxides in the sub-25−30 nm size regime generally exhibit superparamagnetic behavior and quantum confinement effects.[33]

Fe_3O_4 is known to be half-metallic, having full spin polarization and a very high Curie temperature (∼858 K).[34] The magnetoresistance (MR) values reported in literature differ both in magnitude and even in sign, and such discrepancies have been related to the grain structure of the samples.[35] Spin-dependent electron transport and spin-filter effects have been reported for Fe_3O_4 nanowires, where they can be controlled *via* bias voltage and a positive magnetoresistance was observed.[18] Conversely, a negative MR was reported in tunneling junctions of stacked monolayers of Fe_3O_4 NCs.[26] Room-temperature single-electron tunneling (SET) was also observed in case of surfactant-stabilized iron oxide NCs that were presumed to have a Fe_3O_4/γ-Fe_2O_3 core/shell structure with spatially graded composition.[36]

On the other hand, γ-Fe_2O_3 has a band gap dependent on the electron spin, which is at the basis of its spin-filtering properties. Therefore, this material has been proposed to be suitable for magnetic tunnel barriers in room-temperature spin-filter devices.[37,38]

* Address correspondence to giuseppe.maruccio@unisalento.it.

Received for review September 6, 2010 and accepted January 31, 2011.

Published online February 10, 2011
10.1021/nn102301y

In this case, a negative magnetoresistance was recorded and ascribed to field-dependent electron hopping between Fe^{2+} and Fe^{3+} ions (the presence of Fe^{2+} ions should be assumed here).[39] However, such a negative MR could also originate from direct tunneling across γ-Fe_2O_3 particles due to a change in barrier height caused by exchange splitting.[37]

Although magnetotransport through stacked layers of NCs has been previously reported in literature,[26] a few dense-packed superlattice layers of iron oxide NCs sandwiched between two SiO_2 barrier layers represent an interesting case of magnetic tunnel junction (MTJ), which (to our knowledge) has not been investigated so far.

RESULTS AND DISCUSSION

Magnetic Tunnel Junctions. Ordered arrays of magnetic NCs in junction structures can be prepared by physical deposition techniques that can provide desired NC dispersion in template matrices.[12,22] Alternatively, solution casting methods can be used, where deposition of a solution containing monodisperse NCs, followed by solvent evaporation, can result in the self-assembly of thin films made of large-area ordered superlattices.[31,40] In this work, we have investigated MTJs in which a superlattice thin film of organic-capped iron oxide NCs is sandwiched between two Au electrodes. For the first time, we report a switching from negative to positive MR, similar to that recently observed in the case of organic semiconductors.[7,8]

As a representative case of study, we report here the results achieved with MTJ devices incorporating oleate-capped iron oxide NCs with monodisperse ~13 nm size. The NCs were synthesized by a modified two-step seeded-growth protocol based on high-temperature decomposition of $Fe(CO)_5$ in a ternary mixture of oleic acid, oleyl amine, and hexadecane-1,2-diol in 1-octadecene solvent at 280 °C.[41] The bright-field transmission electron microscopy (TEM) overview in Figure 1a demonstrates the high size homogeneity of the as-synthesized NCs (size variance <5%). As a consequence of their elevated monodispersity, the NCs were frequently observed to exhibit a natural tendency to spontaneously organize into two-dimensional ordered superlattices on the TEM grid upon solvent evaporation. This was confirmed by the fast Fourier transform (FFT) pattern calculated for the NC monolayer in Figure 1a, which is indeed compatible with NCs being organized in both cubic and hexagonal close-packed arrangements.[31,40]

As sketched in Figure 2, devices were fabricated as cross-bar structures consisting of Au/SiO_{2-z}/NC film/SiO_{2-z}/Au junctions having areas ranging from 150 to 2400 μm^2 (z denotes vacancies). Since the surfaces of the SiO_2 barriers (patterned in devices) provided the platforms on which the NCs were accommodated, the self-assembly of NCs over such surfaces was

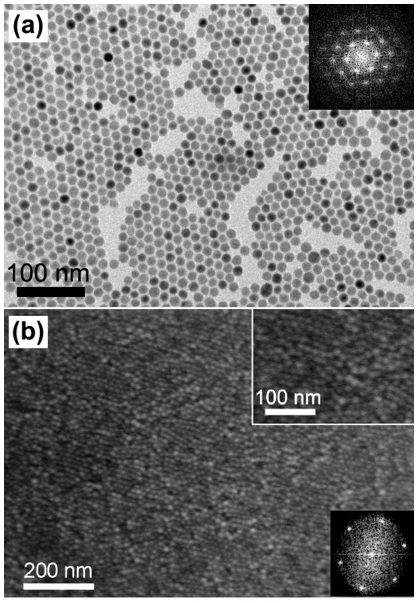

Figure 1. (a) TEM image of 13 nm iron oxide NCs and its fast Fourier transform (FFT) pattern in the inset. (b) SEM images of self-assembled NC superlattice thin films at different magnifications and corresponding FFT pattern. The FFT patterns in panels a and b equally correspond to NCs viewed down the [111] orientation of a cubic phase lattice or down the [001] orientation of a hexagonal phase lattice.

independently investigated by means of scanning electron microscopy (SEM) investigations and optimized for the MTJ fabrication purposes. The number of NC layers and their packing mode in a superlattice depend on the chemical nature and geometric parameters of the NCs concerned, on the deposition conditions, and on the type of substrate used.[31,40] In the present work, large-area superlattice thin films made of a few ordered NC layers stacked on SiO_2 barriers were assembled starting from a concentrated toluene solution of purified NCs by combining the following techniques: (i) an extremely slow solvent evaporation in a quasi-solvent-vapor-saturated ambient[42,43] and (ii) application of an external magnetic field driving the assembly.[32,44] Briefly, for the NC assembly process, a half junction array (*i.e.*, consisting of the back Au electrodes equipped with the SiO_{2-x} barrier layers, as shown in Figure 2a) was immersed into a concentrated toluene solution of iron oxide NCs (Figure 2b), from which the solvent was allowed to evaporate very slowly in saturated atmosphere at room temperature. The deposition of uniform thin films of well-ordered NCs onto the SiO_{2-x} layers was promoted by the application of an external 0.5 T magnet (located underneath the junction array) during the process of solvent evaporation. The high degree of NC monodispersity, combined with the use of a NC solution with a suitable concentration, enabled obtainment of micrometer-scale areas (see Figure S1 of Supporting Information) of compact NC superlattice thin films with thickness ranging from ~40 to ~100 nm, corresponding to 3−8

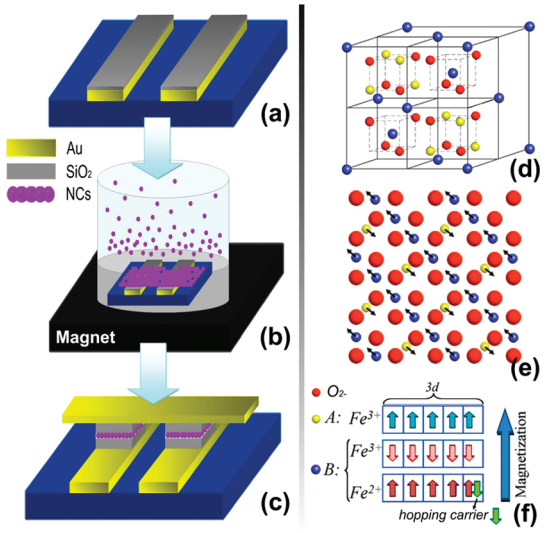

Figure 2. (a−c) Schematic diagram of the MTJ fabrication: (a) first lithography step for the bottom electrodes, (b) NC assembly on the bottom electrodes, (c) second lithography step for the top electrodes and cross-bar configuration of the final MTJs. (d,e) Cubic inverse spinel structure of magnetite: (d) front side of a cubic unit cell with Fe cations occupying interdistances of a fcc-centered cubic closed-packed frame of oxygen ions; (e) corresponding ferrimagnetic organization. (f) Equivalent Fe^{2+} and Fe^{3+} B sites allow charge transfer (or delocalization) and are responsible for magnetite conductivity at room temperature, which is due to hopping of minority spin electrons resulting in a negative spin polarization (due to a spin orientation opposite to the magnetization). Magnetite was reported to behave as a semimetal with a finite density of delocalized states at the Fermi level or a small gap semiconductor.[26] Below T_V, localization of such extravalence electrons leads to a significant drop in conductivity. Maghemite also has a spinel crystal structure but with vacancies in the sites of minority carriers. As a result, maghemite behaves as a disordered semiconductor.

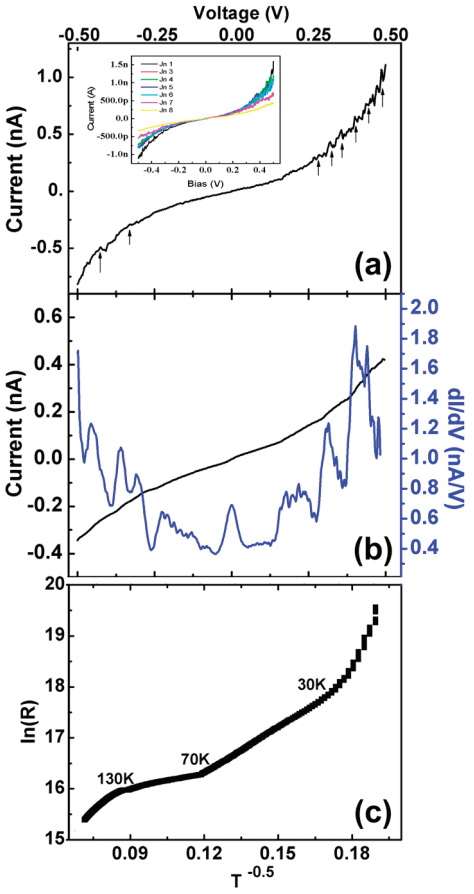

Figure 3. (a) Electron transport at room temperature. $I-V$ pattern shows Coulomb blockade at low voltages and step-like features at higher bias polarity. Not all peaks are marked for clarity. Inset: $I-V$ pattern for eight different junctions (Jn1−Jn8) with area in the range of $30 \times 5\ \mu m^2$ to $30 \times 80\ \mu m^2$ at room temperature with zero magnetic field. (b) $I-V$ curve and dI/dV spectrum for a small area MTJ with few conducting channels. (c) Log R as a function $T^{-0.5}$, showing three different regimes with linear trend as expected for transport controlled by Coulomb blockade in NC superlattices.

layers of 13 nm sized NCs (a cross-sectional SEM view is shown in Figure S2). The degree of ordering achieved can be clearly appreciated from the SEM overview of a typical self-assembled NC superlattice shown in Figure 1b. The corresponding FFT pattern matches with that expected for both cubic and hexagonal close-packed arrangements. After NC superlattice deposition, a new optical lithography step was carried out to define the top electrodes (Figure 2c). Thus, the fabricated MTJ includes, for the first time, a superlattice of magnetic NCs as active layer.

Transport Experiments. Prominent change in current flow is typically expected at specific bias voltages, coupled with single-electron tunneling in case of transport through quantum levels in nanosystems. Single-electron tunneling follows suppression of tunneling current at around zero bias (Coulomb blockade) and step-like behavior at higher voltages (Coulomb staircase) as a consequence of charge accumulation if the resistances associated with the two tunnel barriers are very different.[45] Depending on the nature and quality of the barrier and the interfaces on both sides, the current flow can be significantly asymmetric. With the application of a magnetic field, interplay between single-electron and spin-dependent transport may be observed.[10,11,22,36]

For the present MTJs, room-temperature $I-V$ measurements evidenced nonlinear conduction patterns with a small asymmetry. All $I-V$ curves exhibit similar sigmoidal shapes with higher resistances at small voltages, which can be fitted to a Simmons model for tunneling with similar values of the barrier heights (around 0.30 ± 0.02 eV) and widths (1.3 ± 0.1 nm), which are plausible parameters. The current flow for positive bias is about 1.4 times larger than for the negative polarity side in all junctions. The inset of Figure 3a shows the $I-V$ behavior for a set of junctions with junction area varying from 150 to 2400 μm^2 and current increasing almost linearly with the area. Figure 3a shows a typical $I-V$ curve for a junction with area 1500 μm^2 recorded at room temperature. A number of weak steps marked by arrows are

observable at high voltages. These features can be ascribed to single-electron tunneling through the NC array sandwiched between the two insulating barriers.

At a first assumption, the active region in our MTJs can be approximately described as a granular system. Since the tunneling probability decreases exponentially with increasing barrier width, the roughness of the tunnel barriers should influence transport by locally changing the barrier thickness,[46] as demonstrated by the shorts measured in the case of thinner barriers. As a result, conduction is believed to take place mostly through a number of parallel percolating conduction channels in the MTJ.[26] Each current path may include several interparticle junctions, but those located where the barriers are thinner will dominate transport (similar to hot spots in organic tunnel junctions).[47,48]

When multiple conducting pathways are available within the junction, the conditions for observing a Coulomb staircase are not easily fulfilled, as a large number of channels smear out SET effects. On application of bias voltage, multiple electrons may be trapped inside the array depending on the topology.[49] Ideally, at zero temperature, the system should be insulating and the trapped electrons should lead to a stationary charge state. On increasing the voltage, a transition would occur to a second stable charge configuration *via* a dynamically unstable state. During this transition, current could flow through the junction, leading to charge conduction. Depending upon the number of electrons induced, multiple Coulomb blockade (CB) gaps or stationary charge configurations can arise in steps. At finite temperatures, thermal fluctuations will cause the trapped electrons to tunnel to nearby islands. This would destroy the stable state configuration which could eventually be restored by additional voltage. The process can be repetitive, leading to a nonzero current flow in the multiple Coulomb blockade regions and negative differential resistance behavior in the *I*−*V* pattern, as indeed observed in Figure 3a.

Reducing the contact area leads to the observation of quantum effects since few conducting channels are then available. Coulomb staircase can be better evidenced, and the steps are more precisely identifiable, as seen in Figure 3b, where the *I*−*V* characteristics from a 150 μm^2 sized junction are shown along with the corresponding d*I*/d*V* spectrum. At room temperature, a series of steps and discrete (charging) peaks in the *I*−*V* curve and d*I*/d*V* spectrum, respectively, can be observed. Such patterns are typical of double-tunnel junction structures having dissimilar tunnel barriers. In our case, the bottom SiO_{2-z} layer is deposited on a flat and smooth electrode surface, while the top barrier layer lies on a more uneven NC array that can lead to asymmetry, which is further evidenced at lower temperatures, as shown in Figure 4a. The large slope of the *I*−*V* curve around zero bias with the

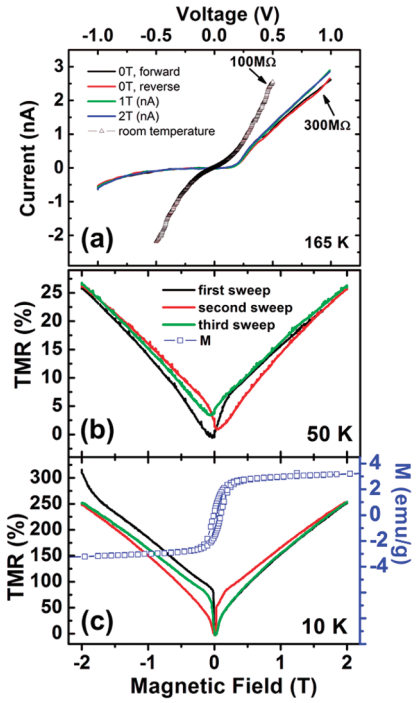

Figure 4. (a) *I*−*V* characteristics from a MTJ at room temperature and 165 K for voltage sweeps at different magnetic field strength. At 165 K, a larger current with increasing magnetic field is observed, corresponding to a negative magnetoresistance of about −5−6%. (b) Positive MR at 50 K and (c) 10 K, along with the NC hysteresis loop (right axis).

corresponding d*I*/d*V* peak around the Fermi level can be related to the metallic phase and the narrow conduction band of magnetite at room temperature.[26] Despite small variations depending on the junction, the voltage separation between adjacent steps in small junctions is around 100 mV. To roughly correlate the capacitance of nanostructure with that of the step size obtained, we can assume domains with a diameter $d = 2r = 13$ nm and calculate $C = 4\pi\varepsilon_0\varepsilon_r r$, where ε_0 and ε_r are the dielectric constant of vacuum and of the tunnel barrier, respectively. Using the values $\varepsilon_r \sim 2-3$,[16] the capacitance obtained is $C = 1.45-2.17$ aF and the estimated Coulomb staircase period is $e/C = 75-110$ mV, a value close to that measured experimentally.

Further confirmation of transport in CB regime comes from the observed $T^{-0.5}$ dependence of resistance on temperature (Figure 3c). Transport in a granular system is typically described by a variable range hopping (VRH) mechanism, according to which the resistance *R* has the following dependence on temperature:

$$R \propto \exp\left\{\left(\frac{T_0}{T}\right)^{\nu}\right\}$$

where ν and T_0 are constants depending on the model considered (Mott or Efros-Shklovskii VRH) and the material properties (density of states and dimensionality).

If mutual Coulomb interactions are taken into account, the density of states near the Fermi level

is parabolically depleted, opening a soft gap, and the Efros-Shklovskii VRH with $\nu = 1/2$ is considered.[50] Tan *et al.*[25] have reported a similar temperature dependence of resistance in CoFe superlattice crystals that show CB at low temperatures in three-dimensional arrays of NCs and a large high-field magnetoresistance (MR). Hopping-type transport between localized states has also been observed in monodispersive arrays of Co@CoO core@shell NCs (model granular systems exhibiting positive MR)[51] as well as in granular Zn-doped Fe_3O_4 polycrystalline materials (the latter show giant tunneling-type MR due to spin polarization in $Zn_xFe_{3-x}O_4$ grains aided by superexchange interaction between different magnetic domains separated by the insulating phase).[52]

In our experimental system, the Efros-Shklovskii VRH well describes the dependence of R on T over the whole temperature range investigated. However, the slope of ln R *versus* $T^{-0.5}$ plot related to the Coulomb gap energy E_c changes significantly. Specifically, at higher temperatures, the calculated E_c is ≈130 meV, while at low temperatures, $E_c \approx 75$ meV. These values fit quite well with those evaluated earlier. At intermediate temperatures, a transition is observed starting at $T_V \sim 120-130$ K, which roughly corresponds to the Verwey transition in Fe_3O_4 associated with localization/delocalization of the extravalence electrons on Fe^{2+}/Fe^{3+} octahedral sites of the spinel crystal structure of magnetite[34] (see also Figure 2d,e). On the basis of the relevant synthesis conditions, the NCs used in the fabricated MTJs can essentially be treated as core/shell objects individually made of an inner half-metallic Fe_3O_4 core domain embedded within a more oxidized γ-Fe_2O_3 shell.[31] While Fe_3O_4 has fluctuating valence states of Fe^{2+} and Fe^{3+} providing electron hopping between them, γ-Fe_2O_3 has vacancies in the sites of minority carriers (Fe^{2+})[18,34,53] and behaves as a disordered semiconductor. As Fe_3O_4 is several orders of magnitude more conductive than γ-Fe_2O_3, the γ-Fe_2O_3 shell (boundary) resistances are the dominant contribution determining the ultimate resistance of NC superlattices above T_V. Below T_V, the extra electrons on Fe^{2+} sites involved in charge transport are frozen/localized and the Fe_3O_4 conductivity drops by 2 orders of magnitude. As a result, below T_V, we expect the contribution of Fe_3O_4 cores to the overall junction resistance to increase. The transition observed in our MTJs may be compared with those in the literature, where the bulk value of $T_V \sim 120$ K was reported to decrease significantly in NCs and for deviations from ideal Fe:O stoichiometry. As a result, the transition may be expected to extend over a large temperature range, due to high surface to volume ratio and off stoichiometry at the surface.[26] The change of relative core/shell contribution to conduction also influences the MR behavior, as described below.

Tunnel Magnetoresistance. The tunnel magnetoresistance in magnetic NCs sandwiched between double-barrier layers (defined as TMR = $(R_H - R_0)/R_0$, where R_0 and R_H are the resistance at zero field and applied field H, respectively) is invariably associated with spin polarization and spin-dependent transport, in addition to single-electron tunneling processes, and gives rise to remarkable TMR phenomena.[9,21,54−57] For NC arrays, the spin transport depends strongly on the particle size effects, the interparticle interactions, and the tunneling regime (either sequential or co-tunneling).[9] TMR is typically negative due to field-induced alignment of the magnetization of adjacent grains. This is the case of Fe_3O_4 single crystals, polycrystalline thin films, pressed powders,[35] but discrepancies in the MR sign were also reported and ascribed to the grain structure of the samples.[35] A negative MR was reported in tunneling junctions of stacked monolayers of Fe_3O_4 NCs, but it decreased to zero around T_V.[26] MR was reported to be anomalously positive in Fe_3O_4 nanowires,[18] certain granular systems, and some magnetic oxide NC arrays.[51] On the other hand, a negative magnetoresistance was reported for γ-Fe_2O_3.[39]

In our junctions, we found a noticeable correlation between the sign of MR and the regimes observed in the temperature dependence of the junction resistance. Specifically, a small MR was measured near 300 K, while ∼5−6% negative MR was observed at 165 K in 2 T magnetic field, as shown in Figure 4a, where the corresponding increase in current with the magnetic field is clearly visible. In this temperature range, the junction resistance is mainly determined by the more resistive γ-Fe_2O_3 shells. Thus, MR is not a bulk phenomenon of Fe_3O_4 cores but is related to tunneling between Fe_3O_4 domains/cores on both sides of γ-Fe_2O_3 shells (boundaries), which leads to a negative MR, depending on the relative orientations of magnetic directions controlled by the magnetic field *via* a domain rotation process. For a granular system, the TMR ratio is often smaller than that calculated according to the Julliére model due to random orientation of the magnetic moments of the grains at zero field.[9] Here

$$\mathrm{TMR} = \frac{m^2P^2}{1 + m^2P^2}$$

where P is the spin polarization and m is the relative magnetization of the granular system.[58] Once saturated ($m = 1$), the relation becomes TMR = $P^2/(1 + P^2)$.[9] When it is assumed that $P \approx 0.5-0.6$ for iron oxide NCs,[34] the resulting TMR is around 20−26%, which is higher than the measured value. However, we should take into account that transport in Fe_3O_4 cores is due to minority spin carriers and the γ-Fe_2O_3 shells act as spin-filter barriers on them (with a higher barrier for spin-down electrons). Moreover, we are still above $T_B \sim 90-100$ K (see Figure S3 in Supporting Information), and NC magnetization is thermally

unstable. Thus, it is reasonable to expect a significant reduction of MR.

The MR then changes sign from negative to positive values across the Verwey transition. At 50 K, TMR is found to be 25−30%, and as the magnetic field is ramped, a significant hysteresis is observed in MR curves for fields ≤80 mT (Figure 4b). These field values are larger than those observed earlier in polycrystalline thin films and pressed powders[35] and can be associated to the NC magnetization based on previously reported magnetic hysteretic behavior in their arrays (Figure 4c). Positive MR values reported in granular systems are often related to various factors, such as curving of carrier trajectories in magnetic fields, shrinkage of localized electronic wave functions, and suppression of hopping paths due to Zeeman splitting of the localized states, depending on the particular case of study.[51] In our junctions, below T_V, the extra electrons are frozen and localized, which is a first reason accounting for positive MR. Additionally, Zeeman splitting of the localized states contributing to carrier hopping can also contribute to positive MR in nanostructured arrays, leading to suppression of spin-dependent transport in the presence of external fields. The exchange coupling between different magnetic domains can enhance the Zeeman splitting of the localized states, leading to large positive MR.[51] On decreasing the temperature further to 10 K, a noteworthy increase in positive TMR is observed that drastically rises up to 300% (Figure 4c). Notably, we observed a good correlation of the low field features in the MR curves with the NC hysteresis loop (Figure 4c). In other words, the MR reflects the NC ferromagnetism. Increasing further the applied magnetic field leads to a minor increase in the magnetization which is accompanied by a more pronounced variation in the MR.

The enhancement of positive MR cannot be explained simply by spin polarization of discrete NCs alone, as the blocking temperature T_B and the tunneling dynamics between adjacent clusters have to be considered. Above $T_B \sim 90-100$ K (see Figure S3), the superparamagnetic moments are thermally unstable and the total magnetization decreases. Below T_B, the magnetization is seen blocked on the time scale of the measurement, and the magnetic moments of the NCs are frozen along their easy axes. For $T > T_B$, the magnetic interactions among cluster domains in nanostructured materials are typically lower, while at low temperatures, they become decisive. In particular, a magnetic exchange energy can arise when magnetic moments are not parallel and electron spin is conserved in tunneling.[52,59] According to Inoue and Maekawa, these magnetic exchange interactions can lead to a large positive MR.[58] Moreover, at very low temperatures, high-order processes of spin-dependent tunneling can play a dominant role in carrier conduction in the attempt of electrons to percolate the superlattice *via* NCs having parallel easy axis and thus preserve their spin. As a result, such processes involving successive tunneling of single electrons also produce MR enhancement, as reported for Co−Al−O granular systems[9] and polycrystalline $Zn_xFe_{3-x}O_4$.[52] Finally, it should be mentioned that, in other works, an enhancement of TMR was related to prominent cotunneling effect in the Coulomb blockade regime, arising from uniform core size and shell thickness.[60]

CONCLUSIONS

In conclusion, a switching from negative to positive TMR has been observed in MTJs sandwiching a superlattice thin film of iron oxide NCs. A good correlation has been found to hold between the magnetoresistance data, the expected magnetism of NC arrays, the charging energies evaluated from $I-V$ curves, and the temperature dependence of their resistance. At low temperatures, a strong enhancement of TMR has also been observed.

EXPERIMENTAL SECTION

Materials. All chemicals were of the highest purity available and were used as received without further purification. Oleic acid ($C_{17}H_{33}CO_2H$ or OLAC, 99%), 1-octadecene ($C_{18}H_{36}$ or ODE, 90%), oleyl amine ($C_{17}H_{33}NH_2$ or OLAM, 70%), iron pentacarbonyl ($Fe(CO)_5$, 98%), and hexadecan-1,2-diol ($C_{12}H_{24}(OH)_2$ or HDIOL, 90%) were purchased from Aldrich. All solvents used were of analytical grade and purchased from Aldrich.

Nanocrystal Synthesis. All of the syntheses were carried out under air-free conditions using a standard Schlenk line setup. Monodisperse oleate-capped iron oxide NCs with variable size were synthesized by a modified two-step seeded-growth protocol based on high-temperature decomposition of $Fe(CO)_5$ in a ODE-diluted OLAC/OLAM/HDIOL mixture at 280 °C.[41] In a typical preparation of 6 nm NCs, 30 g of ODE, 3 mmol of HDIOL, 2 mmol of OLAM, 2 mmol of OLAC, and 4.5 mmol of $Fe(CO)_5$ were comixed and heated up at 15 °C/min to 280 °C and kept at this temperature for 2 h under N_2 atmosphere. To grow larger NCs (up to ∼18 nm in diameter), the required volume (4−10 mL) of an equimolar $FeCO_5$/OLAC solution in ODE (0.5 M) was added dropwise to the crude reaction mixture containing preformed 6 nm NCs at 280 °C, followed by further heating for 2 h under N_2. Finally, the reaction was exposed to air at 80 °C for 1 h to promote oxidation completion.

The NCs were flocculated from their growing mixture upon 2-propanol addition at room temperature and purified upon three cycles of centrifugation and washing with 2-propanol and acetone. Finally, they were fully redissolved in nonpolar solvents (*e.g.*, toluene) for further use.

Device Fabrication. Devices were fabricated as cross-bar structures in the form of double-barrier junctions comprising the following layers: Au/SiO_{2-z}/NC film/SiO_{2-z}/Au, where z denotes vacancies. The junction areas were varied from 150 to 2400 μm^2. Electrodes, supported on Si/SiO_2 wafers, were 100 nm thick

gold lines patterned by optical lithography using a mask aligner. Thin layers of SiO_2 with nominal thicknesses of 3 nm were thermally evaporated on both sides of the NC film to provide adequate electrical insulation (shorts were observed in the case of thinner barriers). To achieve higher-quality tunnel barriers, mild oxygen annealing was performed to reduce vacancies, thus yielding close to stoichiometric SiO_2.

For the NC assembly process, a half junction array (*i.e.*, consisting of the back Au electrodes equipped with the SiO_{2-x} barrier layers, as in Figure 2a) was placed onto the bottom of a 100 mL glass beaker containing 350−400 mL of a 10^{-6} M solution of iron oxide NCs in toluene. The junction array was initially immersed in the liquid (Figure 2b), while the vessel was kept loosely closed in order to permit the internal atmosphere to be saturated with toluene vapors at room temperature. A 0.5 T magnet was located below the beaker. In this way, deposition of uniform thin films of well-ordered NCs onto the SiO_{2-x} layers was promoted under the assistance of the external magnetic field, while the solvent was allowed to fully evaporate over a period of 48−72 h.

Characterization. The Fe atomic content in the NC solutions was measured by inductively coupled plasma atomic emission spectroscopy (ICP-AES) measurements with a Varian Vista AX spectrometer. The samples for analyses were digested in concentrated HNO_3/HCl/(1/3 v/v). The NC concentration was expressed in terms of Fe_2O_3 molecular units.

Low-resolution TEM images of the as-prepared NCs nanocrystals were recorded with a JEOL JEM 1011 microscope operating at an accelerating voltage of 100 kV. The samples for TEM analyses were prepared by dropping a dilute solution of the NRs dissolved in chloroform onto carbon-coated copper grids and then allowing the solvent to evaporate.

High-resolution scanning electron microscopy (HR-SEM) characterization of NCs assembled over substrates was performed with a FEI NOVAnanoSEM200 microscope. Typically, the images were acquired at an accelerating voltage of 5 kV.

Room-temperature current−voltage measurements were performed using a semiconductor parameter analyzer, while low-temperature current and magnetotransport measurements were performed using a cryogen-free magnet (Cryogenic Ltd.).

Acknowledgment. This work was financially supported by the SpiDME European project (sixth Framework Program, NEST, Project No. 029002). The authors thank Benedetta Antonazzo for assistance with SEM measurements. P.D.C. also acknowledges financial support by the Italian Ministry of Education, University and Research through the project AEROCOMP (Contract MIUR No. DM48391).

Supporting Information Available: SEM image of a micrometer-scale area of a compact NC superlattice thin film; cross-sectional SEM image of a magnetic tunnel junction based on iron oxide NC superlattices; temperature-dependent ZFC/FC magnetization curves corresponding to a powder sample of 13 nm iron oxide NCs. This material is available free of charge *via* the Internet at http://pubs.acs.org.

REFERENCES AND NOTES

1. Rocha, A. R.; Garcia-Suarez, V. M.; Bailey, S. W.; Lambert, C. J.; Ferrer, J.; Sanvito, S. Towards Molecular Spintronics. *Nat. Mater.* **2005,** *4*, 335–339.
2. Baadji, N.; Piacenza, M.; Tugsuz, T.; Sala, F. D.; Maruccio, G.; Sanvito, S. Electrostatic Spin Crossover Effect in Polar Magnetic Molecules. *Nat. Mater.* **2009,** *8*, 813–817.
3. Santos, T. S.; Lee, J. S.; Migdal, P.; Lekshmi, I. C.; Satpati, B.; Moodera, J. S. Room-Temperature Tunnel Magnetoresistance and Spin-Polarized Tunneling through an Organic Semiconductor Barrier. *Phys. Rev. Lett.* **2007,** *98*, 016601.
4. Hueso, L. E.; Pruneda, J. M.; Ferrari, V.; Burnell, G.; Valdes-Herrera, J. P.; Simons, B. D.; Littlewood, P. B.; Artacho, E.; Fert, A.; Mathur, N. D. Transformation of Spin Information into Large Electrical Signals Using Carbon Nanotubes. *Nature* **2007,** *445*, 410–413.
5. Petta, J. R.; Slater, S. K.; Ralph, D. C. Spin-Dependent Transport in Molecular Tunnel Junctions. *Phys. Rev. Lett.* **2004,** *93*, 136601.
6. Yoo, J.-W.; Jang, H. W.; Prigodin, V. N.; Kao, C.; Eom, C. B.; Epstein, A. J. Giant Magnetoresistance in Ferromagnet/Organic Semiconductor/Ferromagnet Heterojunctions. *Phys. Rev. B* **2009,** *80*, 205207.
7. Bergeson, J. D.; Prigodin, V. N.; Lincoln, D. M.; Epstein, A. J. Inversion of Magnetoresistance in Organic Semiconductors. *Phys. Rev. Lett.* **2008,** *100*, 067201.
8. Bloom, F. L.; Wagemans, W.; Kemerink, M.; Koopmans, B. Separating Positive and Negative Magnetoresistance in Organic Semiconductor Devices. *Phys. Rev. Lett.* **2007,** *99*, 257201.
9. Yakushiji, K.; Mitani, S.; Ernult, F.; Takanashi, K.; Fujimori, H. Spin-Dependent Tunneling and Coulomb Blockade in Ferromagnetic Nanoparticles. *Phys. Rep.* **2007,** *451*, 1–35.
10. Barnas, J.; Weymann, I. Spin Effects in Single-Electron Tunnelling. *J. Phys.: Condens. Matter* **2008,** *20*, 423202.
11. Seneor, P.; Bernand-Mantel, A.; Petroff, F. Nanospintronics: When Spintronics Meets Single Electron Physics. *J. Phys.: Condens. Matter* **2007,** *19*, 165222.
12. Schelp, L. F.; Fert, A.; Fettar, F.; Holody, P.; Lee, S. F.; Maurice, J. L.; Petroff, F.; Vaurès, A. Spin-Dependent Tunneling with Coulomb Blockade. *Phys. Rev. B* **1997,** *56*, R5747.
13. Bernand-Mantel, A.; Seneor, P.; Lidgi, N.; Munoz, M.; Cros, V.; Fusil, S.; Bouzehouane, K.; Deranlot, C.; Vaures, A.; Petroff, F..;*et al.*Evidence for Spin Injection in a Single Metallic Nanoparticle: A Step towards Nanospintronics. *Appl. Phys. Lett.* **2006,** *89*, 062502.
14. Bernand-Mantel, A.; Seneor, P.; Bouzehouane, K.; Fusil, S.; Deranlot, C.; Petroff, F.; Fert, A. Anisotropic Magneto-Coulomb Effects and Magnetic Single-Electron-Transistor Action in a Single Nanoparticle. *Nat. Phys.* **2009,** *5*, 920–924.
15. Zwanenburg, F. A.; van der Mast, D. W.; Heersche, H. B.; Kouwenhoven, L. P.; Bakkers, E. Electric Field Control of Magnetoresistance in InP Nanowires with Ferromagnetic Contacts. *Nano Lett.* **2009,** *9*, 2704–2709.
16. Black, C. T.; Murray, C. B.; Sandstrom, R. L.; Sun, S. H. Spin-Dependent Tunneling in Self-Assembled Cobalt-Nanocrystal Superlattices. *Science* **2000,** *290*, 1131–1134.
17. Guéron, S.; Deshmukh, M. M.; Myers, E. B.; Ralph, D. C. Tunneling *via* Individual Electronic States in Ferromagnetic Nanoparticles. *Phys. Rev. Lett.* **1999,** *83*, 4148.
18. Liao, Z. M.; Li, Y. D.; Xu, J.; Zhang, J. M.; Xia, K.; Yu, D. P. Spin-Filter Effect in Magnetite Nanowire. *Nano Lett.* **2006,** *6*, 1087–1091.
19. Maruccio, G.; Janson, M.; Schramm, A.; Meyer, C.; Matsui, T.; Heyn, C.; Hansen, W.; Wiesendanger, R.; Rontani, M.; Molinari, E. Correlation Effects in Wave Function Mapping of Molecular Beam Epitaxy Grown Quantum Dots. *Nano Lett.* **2007,** *7*, 2701–2706.
20. Maruccio, G.; Meyer, C.; Matsui, T.; Talapin, D. V.; Hickey, S. G.; Weller, H.; Wiesendanger, R. Wavefunction Mapping of Immobilized Inp Semiconductor Nanocrystals. *Small* **2009,** *5*, 808–812.
21. Barnaś, J.; Fert, A. Magnetoresistance Oscillations Due to Charging Effects in Double Ferromagnetic Tunnel Junctions. *Phys. Rev. Lett.* **1998,** *80*, 1058.
22. Yakushiji, K.; Ernult, F.; Imamura, H.; Yamane, K.; Mitani, S.; Takanashi, K.; Takahashi, S.; Maekawa, S.; Fujimori, H. Enhanced Spin Accumulation and Novel Magnetotransport in Nanoparticles. *Nat. Mater.* **2005,** *4*, 57–61.
23. Tan, R. P.; Carrey, J.; Desvaux, C.; Grisolia, J.; Renaud, P.; Chaudret, B.; Respaud, M. Transport in Superlattices of Magnetic Nanoparticles: Coulomb Blockade, Hysteresis, and Switching Induced by a Magnetic Field. *Phys. Rev. Lett.* **2007,** *99*, 176805.
24. Tan, R. P.; Carrey, J.; Respaud, M.; Desvaux, C.; Renaud, P.; Chaudret, B. High-Field and Low-Field Magnetoresistances of Cofe Nanoparticles Elaborated by Organometallic Chemistry. *J. Appl. Phys.* **2008,** *103*, 07f317.
25. Tan, R. P.; Carrey, J.; Respaud, M.; Desvaux, C.; Renaud, P.; Chaudret, B. 3000% High-Field Magnetoresistance in Super-Lattices of Cofe Nanoparticles. *J. Magn. Magn. Mater.* **2008,** *320*, L55–L59.

26. Poddar, P.; Fried, T.; Markovich, G. First-Order Metal-Insulator Transition and Spin-Polarized Tunneling in Fe3o4 Nanocrystals. *Phys. Rev. B* **2002,** *65*, 172405.
27. Lisiecki, I.; Parker, D.; Salzemann, C.; Pileni, M. P. Face-Centered Cubic Supra-Crystals and Disordered Three-Dimensional Assemblies of 7.5 nm Cobalt Nanocrystals: Influence of the Mesoscopic Ordering on the Magnetic Properties. *Chem. Mater.* **2007,** *19*, 4030–4036.
28. Petit, C.; Taleb, A.; Pileni, M. P. Self-Organization of Magnetic Nanosized Cobalt Particles. *Adv. Mater.* **1998,** *10*, 259.
29. Min, Y. J.; Akbulut, M.; Kristiansen, K.; Golan, Y.; Israelachvili, J. The Role of Interparticle and External Forces in Nanoparticle Assembly. *Nat. Mater.* **2008,** *7*, 527–538.
30. Park, J. I.; Jun, Y. W.; Choi, J. S.; Cheon, J. Highly Crystalline Anisotropic Superstructures *via* Magnetic Field Induced Nanoparticle Assembly. *Chem. Commun.* **2007,** 5001–5003.
31. Pileni, M. P. Self-Assembly of Inorganic Nanocrystals: Fabrication and Collective Intrinsic Properties. *Acc. Chem. Res.* **2007,** *40*, 685–693.
32. Ahniyaz, A.; Sakamoto, Y.; Bergstrom, L. Magnetic Field-Induced Assembly of Oriented Superlattices from Maghemite Nanocubes. *Proc. Natl. Acad. Sci. U.S.A.* **2007,** *104*, 17570–17574.
33. Park, J.; An, K. J.; Hwang, Y. S.; Park, J. G.; Noh, H. J.; Kim, J. Y.; Park, J. H.; Hwang, N. M.; Hyeon, T. Ultra-Large-Scale Syntheses of Monodisperse Nanocrystals. *Nat. Mater.* **2004,** *3*, 891–895.
34. Fonin, M..;*et al.*Magnetite: A Search for the Half-Metallic State. *J. Phys.: Condens. Matter* **2007,** *19*, 315217.
35. Coey, J. M. D.; Berkowitz, A. E.; Balcells, L.; Putris, F. F.; Parker, F. T. Magnetoresistance of Magnetite. *Appl. Phys. Lett.* **1998,** *72*, 734–736.
36. Moore, R. G. C.; Evans, S. D.; Shen, T.; Hodson, C. E. C. Room-Temperature Single-Electron Tunnelling in Surfactant Stabilised Iron Oxide Nanoparticles. *Physica E* **2001,** *9*, 253–261.
37. Wiemann, J. A.; Carpenter, E. E.; Wiggins, J.; Zhou, W. L.; Tang, J. K.; Li, S. C.; John, V. T.; Long, G. J.; Mohan, A. Magnetoresistance of a (Gamma-Fe_2O_3)(80)Ag-20 Nanocomposite Prepared in Reverse Micelles. *J. Appl. Phys.* **2000,** *87*, 7001–7003.
38. Yanagihara, H.; Hasegawa, M.; Kita, E.; Wakabayashi, Y.; Sawa, H.; Siratori, K. Iron Vacancy Ordered Gamma-Fe_2O_3(001) Epitaxial Films: The Crystal Structure and Electrical Resistivity. *J. Phys. Soc. Jpn.* **2006,** *75*, 054708.
39. Tang, J.; Feng, L.; Wiemann, J. A. Negative Magnetoresistance of Gamma-Fe2o3 Observed in Gamma-Fe_2O_3/Ag Granular Nanocomposites. *Appl. Phys. Lett.* **1999,** *74*, 2522–2524.
40. Pileni, M. P. Self-Assembly of Inorganic Magnetic Nanocrystals: A New Physics Emerges. *J. Phys. D: Appl. Phys.* **2008,** *41*, 134002.
41. Cozzoli, P. D.; Snoeck, E.; Garcia, M. A.; Giannini, C.; Guagliardi, A.; Cervellino, A.; Gozzo, F.; Hernando, A.; Achterhold, K.; Ciobanu, N..;*et al.*Colloidal Synthesis and Characterization of Tetrapod-Shaped Magnetic Nanocrystals. *Nano Lett.* **2006,** *6*, 1966–1972.
42. Rizzo, A.; Nobile, C.; Mazzeo, M.; De Giorgi, M.; Fiore, A.; Carbone, L.; Cingolani, R.; Manna, L.; Gigli, G. Polarized Light Emitting Diode by Long-Range Nanorod Self-Assembling on a Water Surface. *ACS Nano* **2009,** *3*, 1506–1512.
43. Talapin, D. V.; Lee, J. S.; Kovalenko, M. V.; Shevchenko, E. V. Prospects of Colloidal Nanocrystals for Electronic and Optoelectronic Applications. *Chem. Rev.* **2010,** *110*, 389–458.
44. Li, L.; Yang, Y.; Ding, J.; Xue, J. Synthesis of Magnetite Nanooctahedra and Their Magnetic Field-Induced Two-/Three-Dimensional Superstructure. *Chem. Mater.* **2010,** *22*, 3183–3191.
45. Maruccio, G.; Wiesendanger, R. Scanning Tunneling Spectroscopy of Semiconductor Quantum Dots and Nanocrystals. In *Quantum Materials, Lateral Semiconductor Nanostructures, Hybrid Systems and Nanocrystals*; Heitmann, D., Ed.; Springer: Berlin, Heidelberg: 2010; pp 183−216.
46. Maruccio, G.; Marzo, P.; Krahne, R.; Passaseo, A.; Cingolani, R.; Rinaldi, R. Protein Conduction and Negative Differential Resistance in Large-Scale Nanojunction Arrays. *Small* **2007,** *3*, 1184–1188.
47. Barraud, C.; Seneor, P.; Mattana, R.; Fusil, S.; Bouzehouane, K.; Deranlot, C.; Graziosi, P.; Hueso, L.; Bergenti, I.; Dediu, V..; *et al.*Unravelling the Role of the Interface for Spin Injection into Organic Semiconductors. *Nat. Phys.* **2010,** *6*, 615–620.
48. Sanvito, S. Molecular Spintronics the Rise of Spinterface Science. *Nat. Phys.* **2010,** *6*, 562–564.
49. Shin, M.; Lee, S.; Park, K. W.; Lee, E. H. Coulomb Blockade Gap and Coulomb Staircase of a New Type in Various Tunnel-Junction Arrays with Two Branches. *Superlattices Microstruct.* **1999,** *25*, 279–284.
50. Kim, J.-J.; Lee, H. J. Observation of a Nonmagnetic Hard Gap in Amorphous in/Inox Films in the Hopping Regime. *Phys. Rev. Lett.* **1993,** *70*, 2798.
51. Xing, H.; Kong, W. J.; Kim, C. H.; Peng, S.; Sun, S. H.; Xu, Z. A.; Zeng, H. Giant Positive Magnetoresistance in Co@Coo Nanoparticle Arrays. *J. Appl. Phys.* **2009,** *105*, 063920.
52. Chen, P.; Xing, D. Y.; Du, Y. W.; Zhu, J. M.; Feng, D. Giant Room-Temperature Magnetoresistance in Polycrystalline $Zn_{0.41}Fe_{2.59}O_4$ with Alpha-Fe_2O_3 Grain Boundaries. *Phys. Rev. Lett.* **2001,** *87*, 107202.
53. Hu, G.; Suzuki, Y. Negative Spin Polarization of Fe_3O_4 in Magnetite/Manganite-Based Junctions. *Phys. Rev. Lett.* **2002,** *89*, 276601.
54. Graf, H.; Vancea, J.; Hoffmann, H. Single-Electron Tunneling at Room Temperature in Cobalt Nanoparticles. *Appl. Phys. Lett.* **2002,** *80*, 1264–1266.
55. Himpsel, F. J.; Ortega, J. E.; Mankey, G. J.; Willis, R. F. Magnetic Nanostructures. *Adv. Phys.* **1998,** *47*, 511–597.
56. Tinkham, M.; Davidovic, D.; Ralph, D. C.; Black, C. T. Tunneling through Metallic Quantum Dots. *J. Low Temp. Phys.* **2000,** *118*, 271–285.
57. Zeng, H.; Li, J.; Liu, J. P.; Wang, Z. L.; Sun, S. Exchange-Coupled Nanocomposite Magnets by Nanoparticle Self-Assembly. *Nature* **2002,** *420*, 395–398.
58. Inoue, J.; Maekawa, S. Theory of Tunneling Magnetoresistance in Granular Magnetic Films. *Phys. Rev. B* **1996,** *53*, R11927.
59. Helman, J. S.; Abeles, B. Tunneling of Spin-Polarized Electrons and Magnetoresistance in Granular Ni Films. *Phys. Rev. Lett.* **1976,** *37*, 1429.
60. Peng, D. L.; Sumiyama, K.; Konno, T. J.; Hihara, T.; Yamamuro, S. Characteristic Transport Properties of Coo-Coated Monodispersive Co Cluster Assemblies. *Phys. Rev. B* **1999,** *60*, 2093.